An optimized fully-atomistic procedure to generate glassy polymer films for molecular dynamics simulations

Sylvie Neyertz, David Brown

Version of Record: https://www.sciencedirect.com/science/article/pii/S0927025619307980
Manuscript_4ef3dbf8f6c46dca910963618feba95d

An Optimized Fully-Atomistic Procedure to Generate Glassy Polymer Films for Molecular Dynamics Simulations

Sylvie NEYERTZ* and David BROWN

Univ. Savoie Mont Blanc, Univ. Grenoble Alpes, CNRS, Grenoble INP, LEPMI, 38000 Grenoble, France

*Corresponding author: sylvie.neyertz@univ-smb.fr, postal address: LEPMI(LMOPS), CNRS UMR 5279, Univ. Savoie Mont Blanc, Bât. Hélios, Savoie Technolac, 73376 Le Bourget du Lac Cedex, France

Graphical abstract

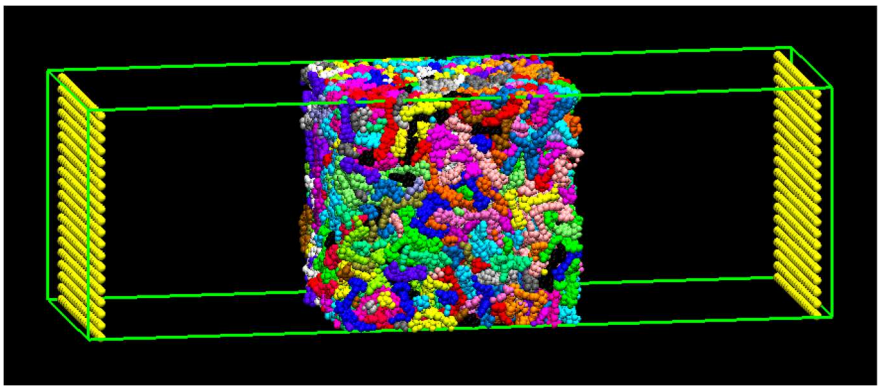

Abstract

An explicit-atom wall-compression procedure has been optimized in order to generate glassy polymer films containing both surface-like and bulk-like chains for use in molecular dynamics (MD) simulations. All steps are carried out at the fully-atomistic level, which avoids the complexities of coarse-graining and back-mapping. One dimension of an isotropic bulk MD box is extended and walls are placed at both ends of the enlarged simulation box. The walls progressively advance towards the polymer at a slow rate until the resulting film regains a bulk-like density in its core. Following local relaxation at moderate and high temperatures, the walls are pushed back to the edges of the simulation box and the free-standing glassy film is allowed to relax. The 6FDA-6FpDA, 6FDA-6FmDA and 6FDA-DAM polyimides were chosen as test cases. The effects of the chain lengths, the rate of wall compression, the temperatures as well as the conditions of the simulations were assessed by monitoring the densities, conformations and configurations of the chains at each step. The optimized procedure leads to surface

chains being aligned and flattened with respect to the interfaces, while the bulk chains in the centre of the models remain unaffected. Molecular models of glassy polymer films containing ~80000 atoms with an isotropic core of volume ~(60×100×100) $Å^3$ and two interfacial regions, each of volume ~(20×100×100) $Å^3$, were created. As found before for simpler models, the interfacial width is of the order of the average radius of gyration of the chains.

Keywords

molecular dynamics (MD) simulations, glassy polymers, films, membranes, optimization, polyimides

1. Introduction

Polymer membranes are involved in a large number of high-performance applications related to the selective transport of small ions or molecules, e.g. gas separation, water purification, fuel cells or batteries. However, their structure-property relationships are not easy to comprehend and it is often useful to complement experimental characterizations by molecular modelling techniques such as molecular dynamics (MD) simulations [1]. These provide detailed information at the molecular level, and can even be used as a pre-screening tool before undertaking new membrane developments [2, 3].

A standard MD simulation integrates Newton's equations of motion for all the atoms in a system. The timestep has to be smaller than the timescale of the fastest vibrations in order to properly represent the dynamics of the system under study [4]. In explicit-atom polymer simulations, a stable integration with satisfactory energy conservation in the microcanonical *NVE* ensemble (constant number of atoms *N*, constant volume *V*, constant total energy *E*) is usually obtained using a timestep of $\Delta t = 10^{-15}$ s. While there are higher-frequency modes such as bond stretching or fast motions of the hydrogens in explicit CH, CH_2 and CH_3 groups, these can be taken into account by using rigid constraints [5, 6]. Electrostatic interactions are particularly time-consuming as elaborate techniques such as the Ewald summation [7] have to be used. These interactions can be temporarily switched off during the preparation steps for polymer structures [8], but charges cannot be ignored for most properties [2, 9, 10]. Integrations are typically carried out over 1-100 million timesteps, and consequently, fully-atomistic simulations (including electrostatic interactions) are currently restricted to the 10^{-9}-10^{-7} s timescale. Indeed, standard explicit-atom polymer MD simulations are of the order of 1-20 ns [11-14] Even if longer simulations of 100-300 ns have been reported [2, 8], they remain few up to now. In all cases, MD timescales are hardly compatible with the relaxation phenomena associated to molecular disentanglements and translations of polymer chains, which can reach the order of 1 s or more [15, 16].

Another limitation is the system size that can be modelled. These are usually in the range of 5000-20000 atoms for fully-atomistic representations [14, 17-20]. There again, larger models of up to 150000 atoms have been reported, but simulations had to be carried out over many months [21-24]. MD box sizes thus remain very small compared to the real materials. Edge effects can be removed by implementing periodic boundary conditions, which replicate the primary box in all three dimensions while conserving

its number density. This effectively makes the system infinite in all directions and removes most of the size effects for systems as small as ~(25-30) $Å^3$ [18]. In polymer simulations, such bulk models are deemed as being representative of the membrane core. On the other hand, it is necessary to prepare films containing actual surfaces in order to describe phenomena associated with the interfacial parts of a membrane, *e.g.* gas sorption in a polymer [24-26]. Unless other techniques (such as *e.g.* Monte Carlo simulations [27, 28]) are being used, the simplest way in MD simulations is to extend one of the box axes in order to create an empty space on both sides of a polymer bulk. The boundary conditions along this direction can then be removed to prevent interactions of the parent chains with their images [29-31]. In principle, this should allow for the macromolecules close to the interfaces to relax from bulk-like to surface-like structures. However, in reality, this is only possible for flexible and very short molecules. Indeed, polymer glasses have been described as "inherently configurationally-arrested" and "characterized by immeasurably small chain self-diffusivities" [32, 33]. The problem is illustrated by Fig. 1, which is based on a 10-monomer 6FDA-6FpDA polyimide bulk prepared at 308 K as described in Ref. [19]. At time $t = 0$, the box of the bulk model is extended along the x direction to create empty spaces (Fig. 1 (a)). Fig. 1 (b) displays the same system following a 5 ns MD simulation under *NPT* (constant number of atoms N, pressure P and temperature T) conditions.

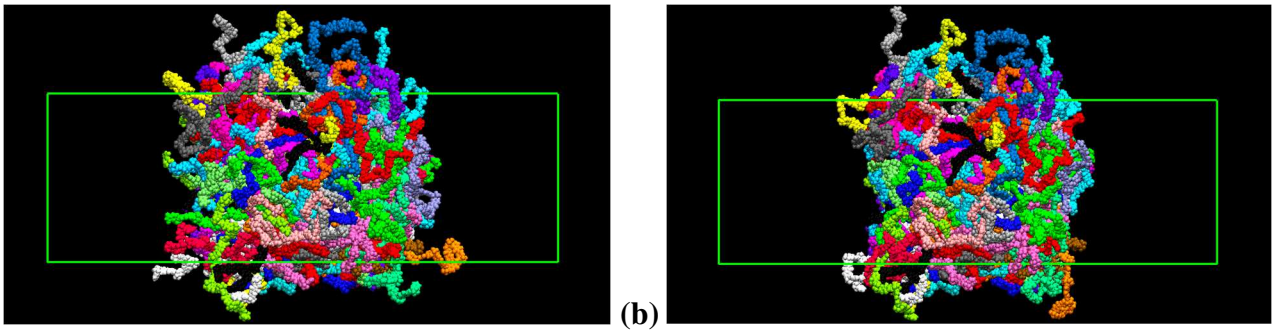

Fig. 1. Schematic representations of a bulk polyimide with its MD simulation box being extended along the x-axis (full box x-length: ~300 Å). The system is shown at **(a)** $t = 0$ ns and **(b)** $t = 5$ ns. The software for display is VMD (Visual Molecular Dynamics) [34] and the different colours refer to the different chains.

It is clear from Fig. 1 that, even at the interfaces, such low-mobility molecules are simply unable to relax more than on the very local level under the MD timescale. At higher temperatures, *e.g.* at 650 K,

the average mean-square radius of gyration of the chains $\langle S^2 \rangle$ changes by less than 5% over 5 ns (results not shown). High-temperature relaxations can be more efficient for flexible polymers such as polybutadiene but they are not recommended either as the films tend to lose their cohesion in the centre [30].

It is possible to coarse-grain the bulk model, increase the box axis and remove the boundary conditions in one direction, relax the film in the coarse-grained form and finally map it back to the fully-atomistic scale [28, 35-37]. This multiscale approach is a lot more satisfactory than the previous one but, unfortunately, the initial parametrization and the reverse mapping procedures are very complex, structure-specific and difficult to optimize [38-40]. Another alternative is the fully-atomistic wall-compression which was loosely inspired by the experimental solvent-casting procedure [2, 21-26, 41, 42]. All steps are carried out at the explicit-atom level, which avoids the complexities of coarse-graining and back-mapping. The wall-compression approach mimicks the solvation step followed by the evaporation of the solvent by extending one axis of an MD box containing a bulk melt, placing structureless flat repulsive walls perpendicular to this axis at each edge of the simulation box and advancing progressively the walls towards the polymer at a very slow rate until it regains its density in the middle of the film. Although solvent evaporation has been simulated for coarse-grained bead-spring models [43], the solvent cannot be not explicitly simulated in explicit-atom simulations of large chain molecules as the very significant increase in the number of atoms is prohibitive in terms of computational times. The wall-compression technique has already been applied to several glassy polyimides containing 40-50 monomers *per* chain [2, 21-26, 41, 42]. The chain structures in the vicinity of the interfaces flattened and favoured a parallel orientation with respect to the surfaces. This agrees with surface-layer chains reported for films of more flexible and/or much shorter polymers as well as simplified models, which were fully equilibrated over their generation procedure [28, 29, 35, 44-46]. In addition, the flattened/parallel to the surface nature of free-standing chain structures are known to be similar (albeit attenuated) to those of polymers in the vicinity of a solid interface [44, 45, 47-50]. Even if equilibrated coarse-grained chains in supported films tend to exhibit a clear density layering and less mobility than those in free-standing films [45, 46, 50, 51], the presence of walls should thus not lead to unrealistic structures. However, the main drawback of the glassy 40-50-mers polyimide model films was that the surface features of the chains extended up across

the whole models, even if they were quite attenuated in the centres. As such, bulk models had to be run separately to truly represent the membrane cores [19, 52].

The present work significantly improves the wall-compression procedure in order to generate fully-atomistic glassy polymer films containing ***both*** surface-like and bulk-like chains for use in MD simulations. Several factors, *i.e.* the length of the chains, the rate of wall compression, the temperatures as well as the conditions of the simulations have been optimized. The test cases are three glassy polyimide structures based on the 6FDA dianhydride [53], *i.e.* the 6FDA-6FpDA and 6FDA-6FmDA structural isomers along with the lower density 6FDA-DAM. All three chemical formulae are given in Fig. 2. For simplicity, they will be referred to in the text as PI1, PI2 and PI3, respectively.

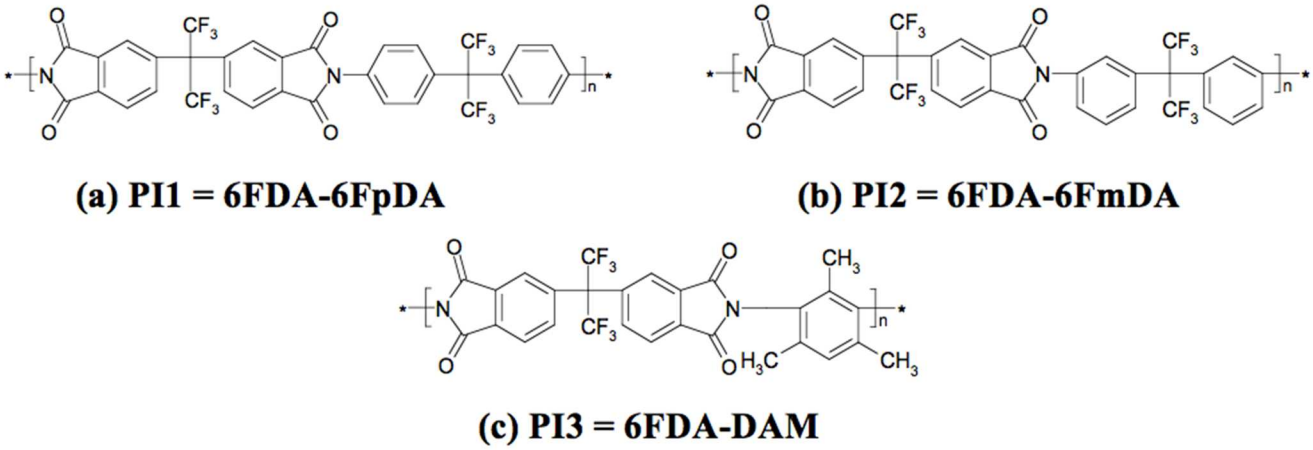

Fig. 2 Chemical structures of the glassy polyimides used as test cases. In the monomers, the dianhydride-derived fragment is 6FDA and the diamine-derived fragments are 6FpDA for PI1, 6FmDA for PI2 and DAM for PI3, respectively.

Although model films of both isomers have already been used to study various aspects of CO_2 permeation at 308 K [2, 24-26], these were mainly representative of the surface layers. We now show that the newly-optimized procedure still gives realistic models of glassy films, but with both surface and bulk chains being accounted for.

2. Optimization of the generation procedure for polymer films

2.1. The fully-atomistic force-field

All simulations were carried out using the parallelized *gmq* package [54]. In an explicit-atom MD force-field, polymer chains are usually described by several "bonded" potentials representing the angle-bending, torsional and out-of-plane interactions, as well as by two "nonbonded" potentials describing the excluded-volume and electrostatic interactions [1, 4]. Furthermore, it is highly recommended to remove high-frequency motions such as bond stretching and the hydrogens motions in explicit CH, CH_2 and CH_3 groups by using special constraints [5, 6]. This allows for the use of a reasonable time-step of 10^{-15} s in the integration algorithm, while ensuring a proper equipartition of the kinetic energy.

The classical force-field used here [54] is the sum of all the bonded and nonbonded potentials (Eq. (1)):

$$U_{pot} = \sum_{\theta} U_{bend}(\theta) + \sum_{\tau} U_{tors}(\tau) + \sum_{i-planar} U_{oop}(i) + \sum_{(i,j)nb} U_{vdw}(r) + \sum_{(i,j)nb} U_{coul}(r) \qquad (1)$$

In Eq. (1), the angle-bending deformations are described by a harmonic function in the cosine of the bond angles θ:

$$U_{bend}(\theta) = \frac{k_\theta}{2}(\cos\theta - \cos\theta_0)^2 \qquad (2)$$

where k_θ is a constant determining the flexibility of the angle and θ_0 is the equilibrium bond angle. The torsional motions around the dihedral angles τ are represented by a third-order polynomial in $cos\,\tau$:

$$U_{tors}(\tau) = \sum_{n=0}^{3} a_n \cos^n \tau \qquad (3)$$

with the dihedral angle τ varying from -180° to +180°, $\tau = 0°$ being the *trans* conformation and a_n being the torsional coefficients. The out-of-plane term keeps sp^2 structures planar by using a harmonic function in the perpendicular distance d from the central atom i to the plane defined by its three attached atoms with k_{oop} being the force constant:

$$U_{oop}(i) = \frac{k_{oop}}{2} d^2 \qquad (4)$$

The fourth and fifth terms of Eq. (1) are the nonbonded potentials, which depend on the distance r between two interacting sites. These are applied to all atom pairs situated either on the same chain but separated by more than two bonds or on two different chains. The van der Waals interactions are described by the common 12-6 Lennard-Jones (LJ) form (Eq. (5)):

$$U_{vdw}(r) = U_{LJ}(r) = 4\varepsilon\left[\left(\frac{\sigma}{r}\right)^{12} - \left(\frac{\sigma}{r}\right)^{6}\right] \tag{5}$$

where ε is the well-depth of the potential and σ is the distance at which the potential is zero. The electrostatic or Coulombic potential is given by Eq. (6), with q_i and q_j being the partial charges on atoms i and j respectively, and ε_0 being the vacuum permittivity:

$$U_{coul}(r) = \frac{q_i q_j}{4\pi\varepsilon_0 r} \tag{6}$$

For the polyimides under study, the interaction parameters were taken from the TRIPOS 5.2 generic force field [55] and the partial charges were obtained from density functional theory (DFT) calculations on representative fragments [19]. All other simulation details have already been given [2, 19, 24-26, 56, 57]. As such, we will only describe afterwards the parameters specific to the generation procedure.

2.2. Selection of chain lengths

It has been shown using simpler models that the influence of a membrane interface extends at least over a distance corresponding to 1-1.5 times the average radius of gyration of the chains $\langle S^2 \rangle^{1/2}$ [27, 32, 44, 47, 50]. The width of a film should thus be larger than two to three times $\langle S^2 \rangle^{1/2}$ in order to ensure bulk-like behaviour in its central part. In addition, its transversal dimensions should be of the same order of magnitude than its longitudinal dimension if the system is not expected to present specific anisotropic features such as *e.g.* nanopores. In terms of number of atoms, this can rapidly become critical for dense systems.

The average mean square radius of gyration $\langle S^2 \rangle$ and end-to-end distance $\langle R^2 \rangle$ of the chains were sampled here as a function of the chain length using the hybrid pivot Monte Carlo-molecular dynamics (PMC-MD) procedure, which allows for chain configurations characteristic of the equilibrium melt to be created at a preset temperature [18, 19, 42, 52]. In this approach, the configurational phase-space of the

polymer is sampled in the melt using pivot Monte Carlo (PMC) moves for rotatable torsions [58], while standard MD algorithms are used to explore the oscillatory modes of the chains. Since long-range interactions in pure polymer melts are largely screened out [59], their configurations can be described by considering isolated molecules with only a limited number of specific near-neighbour intramolecular interactions [60], *i.e.* those between atoms separated by 4 backbone bonds for polyimides [19]. As such, the PMC-MD sampling procedure is highly efficient. For glassy polymers, it is preferable to sample just above the Tg, since the configurations should be close to those expected for the lower-temperature glass. The experimental Tg, measured using differential scanning calorimetry (DSC) at heating rates of 10°C/min or 20°C/min, are known to fall in the ranges of 575-605 K for PI1 and 640-670 K for PI3, while it is ~530 K for PI2 [19, 61]. As such, the sampling temperatures were set to 650 K for PI1, 600 K for PI2 and 700 K for PI3. PMC-MD runs were carried out for up to 10000 ps with the number of monomers n in the chain (Fig. 2) ranging from 1 to 50. Monte Carlo pivot moves were attempted every 100 fs. The first 1000 ps of the runs were discarded in order to fully decorrelate the chains from their starting structures [52].

While a smaller radius of gyration will decrease the required number of atoms in the film model, it should still be representative of macromolecular materials. To ensure that the choice of chain lengths does not lead to any size effects, the mean square end-to-end distance $\langle R^2 \rangle$ can be normalized by the number of monomers and by the square of the "length" of a monomer l. A plot of $\langle R^2 \rangle / nl^2$ versus n should thus correspond to a characteristic ratio [59], and only chain lengths associated to its plateau should be selected. For the polyimides under study, l was defined as the average distance between the central carbons of successive 6FDA fragments over the PMC-MD runs at their respective temperatures [19], *i.e.* l = 18.5 Å for PI1, l = 16.8 Å for PI2 and l = 15.2 Å for PI3. Fig. 3 presents the average radius of gyration $\langle S^2 \rangle^{1/2}$ (left axis) along with the mean square end-to-end distance normalized by the length of the chain, $\langle R^2 \rangle / nl^2$ (right axis), for both PI1 (Fig. 3 (a)) and PI3 (Fig. 3 (b)).

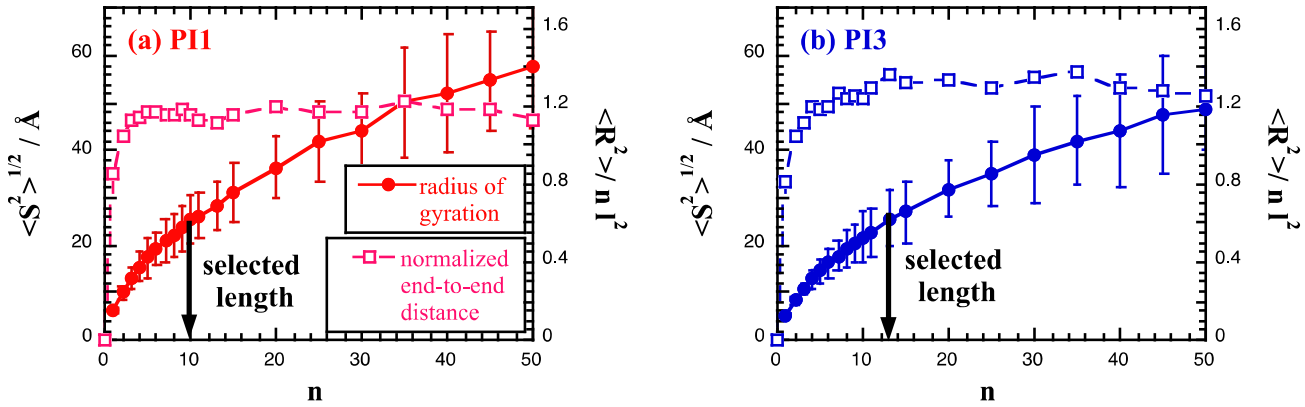

Fig. 3 Average radius of gyration along with its standard error (full symbols, left axis) and average mean square end-to-end distance normalized by the chain length (empty symbols, right axis) as a function of the number of monomers n in a chain sampled by PMC-MD for **(a)** PI1 at 650 K and **(b)** PI3 at 700 K. The legend is the same for both graphs and the maximum standard error on the $\langle R^2 \rangle / nl^2$ is 0.12.

Although several choices are available for the chain lengths (Fig. 3), the value of n corresponding to an average radius of gyration of ~25 Å was selected in the present work in order to build membranes of ~(100 Å)^3, *i.e.* four times as wide as $\langle S^2 \rangle^{1/2}$, and with two surface areas of ~10000 Å^2. This corresponded to chain lengths of 10 monomers (662 atoms) for both PI1 and PI2 isomers and 13 monomers (730 atoms) for PI3.

2.3. Isotropic bulk models

The number of chains to consider for a ~(100 Å)^3 bulk was evaluated from the average experimentally-reported densities, i.e. 1477±3 kg m^{-3} for PI1, 1493±1 kg m^{-3} for PI2 and 1339±7 kg m^{-3} for PI3 [19]. This amounted to 120 chains (79440 atoms) for both PI1 and PI2 isomers and to 110 chains (80300 atoms) for PI3. As noted above, these are very large systems in terms of fully-atomistic MD.

For each polyimide, a bulk melt model was constructed by generating all the chains using PMC-MD sampling at its preset temperature (just above its T_g, see Section 2.2.), randomly reorientating them and distributing them in a periodic cubic MD box at a density corresponding to the average experimentally-reported value. Since single-chain sampling ignores all "non-local" interactions, the PMC-MD-selected structures usually have large overlap energies. These are easily removed *via* the progressive introduction of the excluded-volume under *NVT* (constant number of atoms N, volume V and temperature

T) conditions. An additional difficulty with cyclic molecules is that a bond can become trapped with the two atoms of the bond on either side of a ring or, alternatively, different rings can be interlocked [52]. This is a well-known artefact [62], which can be prevented by adding extra interactions such as "phantom atoms" at the centre of each ring upon completion of the PMC-MD sampling. Following the introduction of the excluded-volume potential, phantom atoms are removed and the electrostatic interactions switched on. Each bulk simulation continued under *NVT* conditions for 5000 ps in order to relax the hot-spots and to allow the melt to come to thermal equilibrium. Temperature was maintained by loose-coupling to a heat bath [63] with a constant of 0.1 ps. The melt was then cooled down to 308 K at a rate of -1 K ps^{-1}. Following a short constant-volume 200 ps simulation at 308 K, the bulk model was switched to constant-pressure *NPT* conditions, *i.e.* the box was allowed to relax freely towards its equilibrium shape and size. The runs continued until the density and other properties stabilized, *i.e.* typically up to 5000 ps. The analyses were carried out on the last 2000 ps.

All three systems remained quasi-cubic, and their relaxed densities were found to settle to 1499.9±0.1 kg m^{-3} for PI1, 1512.3±0.2 kg m^{-3} for PI2 and 1323.0±0.1 kg m^{-3} for PI3. This is within less than 1.6 %, 1.3% and 1.2% of their average experimental values, respectively, which is a strong validation for the choice of potential and the preparation procedure. A schematic representation of the PI3 bulk polymer in its unfolded coordinates is provided in Fig. 4 (a). The 110 chains are displayed in different colours and the boundary conditions ensure that all atoms falling outside the primary MD box have periodic images inside. These systems are thus clearly rather dense.

Conformational isotropy can be assessed by calculating the second-order Legendre functions, $P_2(\cos\theta_\alpha)$, where θ_α is the angle between the α-axis and the vector between atoms *i* and *k* in a {*i*, *j*, *k*} bending angle [21-23, 25, 41, 42]. The P_2 functions are defined with respect to θ_α as:

$$P_2(\cos\theta_\alpha) = \frac{3}{2}\langle\cos^2\theta_\alpha\rangle - \frac{1}{2} \tag{7}$$

If α is the longitudinal direction in a film, the limiting values of $P_2(\cos\theta_\alpha)$ will be -1/2 for an alignment of the angles parallel to the surface (θ_α = 90°, *i.e.* the angles are perpendicular to the vector normal to the surface), 1 for an alignment perpendicular to the surface and 0 for a random alignment. This is similar to the order parameter analyses carried out to characterize the preferential orientations of bonds [27, 28, 35]. In an isotropic bulk, the $P_2(\cos\theta_\alpha)$ should remain all close to zero, irrespective of α being defined as *x*, *y*

or z. The Legendre polynomials were calculated in different slabs and in all three directions for all pivot bending angles in the structures. If Car represents an aromatic carbon and Cket a ketone carbon, the key pivot angles are the Car-C-Car between the aromatic rings, the dianhydride-diamine Cket-N-Car linkers, as well as the CF_3-C-CF_3 angles (Fig. 2). The $P_2(\cos\theta_\alpha)$ defined with respect to the film centre-of-mass (COM) situated at $x = 0$ and averaged over x-slabs of length 10 Å are shown for all the pivot angles of the PI1 bulk models on the left axis of Fig. 4 (b). The slab-mass density of the polymer, $\rho(x)$, averaged over x-slabs of length 2 Å is also displayed as an eye guide on the right axis. Fig. 4 (b) clearly shows that all pivot angles are aligned in a random order along the x direction. Similar plots were obtained using $\alpha = y, z$, *i.e.* the bulk melts were truly isotropic from a conformational point-of-view.

(a) 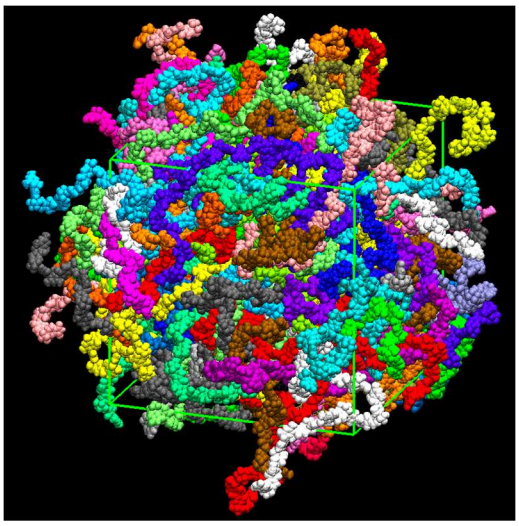

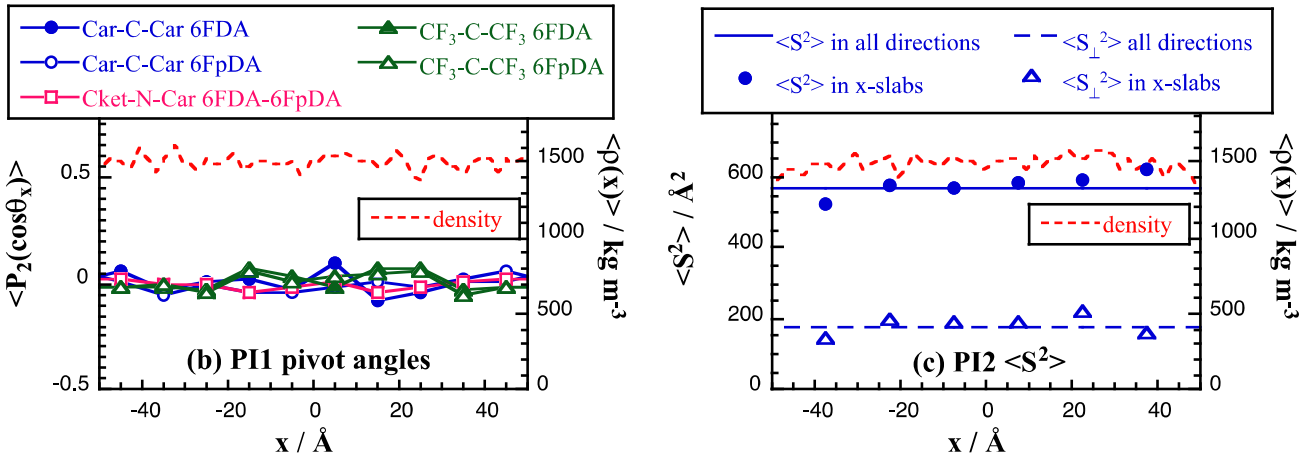

Fig. 4. **(a)** A schematic representation of the PI3 80300-atom bulk at 308 K in its unfolded coordinates **(b)** Left axis: the $\langle P_2(\cos\theta_x)\rangle$ for the PI1 bulk pivot as a function of the distance from the middle angle atom to the total COM averaged over x-slabs of width 10 Å. **(c)** Left axis: the mean-square chain radii of gyration $\langle S^2\rangle$ and its perpendicular $\langle S_\perp^2(x)\rangle$ component averaged over all bulk PI2 chains (lines) along with their values as a function of the distance of the chains COM to the total COM averaged over x-slabs of width 15 Å (symbols). The maximum standard errors are 0.01 on the $\langle P_2(\cos\theta_x)\rangle$, 10 Å^2 on the slab $\langle S^2\rangle$ and 7 Å^2 on the slab $\langle S_\perp^2(x)\rangle$. Also shown for comparison in (**b-c**) are the mass densities $\langle\rho(x)\rangle$ of the polymers averaged over x-slabs of width 2 Å (right axes).

To assess configurational isotropy, properties scanning a larger-scale have to be examined. As before [24], a useful approach is to resolve the average mean-square chain radii of gyration $\langle S^2\rangle$ into slabs spanning $\alpha = x$, y or z and calculate their respective perpendicular components $\langle S_\perp^2(\alpha)\rangle$. If the system is isotropic, $\langle S^2(\alpha)\rangle$ along the α axis should be approximately equal to the total $\langle S^2\rangle$ and both $\langle S_\perp^2\rangle$ and $\langle S_\perp^2(\alpha)\rangle$ should be 1/3 of the total $\langle S^2\rangle$ [64]. Since the number of chains is necessarily limited, this has to be resolved on larger slabs, *e.g.* of width 15 Å. The total $\langle S^2\rangle$ and its perpendicular component $\langle S_\perp^2\rangle$ averaged over all three dimensions, along with their corresponding x-slabs values are displayed for the bulk PI2 chains in Fig. 4c. Similar plots were obtained if $\alpha = y$, z. Within the large error bars due to the limited statistics on the number of chains, $\langle S^2(\alpha)\rangle \approx \langle S^2\rangle$ and $\langle S_\perp^2(\alpha)\rangle \approx \langle S_\perp^2\rangle \approx 1/3\langle S^2\rangle$. This confirms that the bulk models are isotropic from a configurational point-of-view as well.

2.4. Wall compression

The wall compression step was carried out at 308 K. Compressing at higher temperatures leads to a loss of cohesion for chains in the core, and such glassy models are not able to redensify properly over the cooling timescale currently accessible to an explicit-atom MD simulation. For the temperature, it is thus important to find a compromise between too much mobility (that will destroy the cohesion of the entire membrane) and enough mobility for the chains to be able to rearrange at the interfaces. Another remark is that initial tests aimed at generating configurations with PMC-MD sampling in the presence of walls led to non-homogeneous density distributions of the chains (depending on whether the walls were repulsive or attractive), which cannot be either relaxed on the MD timescale. As such, the walls were placed after the isotropic bulk was generated (Section 2.3.). For each bulk, the *x*-axis was extended with respect to the polymer centre-of-mass to ±150 Å and a flat soft-repulsive wall was placed on both sides perpendicular to the *x*-edges of the simulation box at $x_{wall} = \pm 100$ Å. In their unfolded coordinates, a few chains extended out up to $x \approx \pm 75$ Å (Fig. 4 (a)). Setting x_{wall} at ±100 Å thus ensured that the walls were far enough to avoid any initial interactions with the polymer, while still being within a reasonable distance from the polymer. Each wall was defined to be a smoothly decaying soft-repulsive barrier by applying the harmonic potential U_{wall} to any atom *i* whose absolute *x*-position became greater than x_{wall} (Eq. (8)):

$$U_{\text{wall}}(x_i) = \frac{1}{2} k_{\text{wall}} \left(|x_i| - x_{wall} \right)^2 \qquad if \ |x_i| > x_{wall} \tag{8}$$

with the force constant k_{wall} being set to 50 kg s^{-2}. In addition, the forces originating from U_{wall} were limited by an upper bound corresponding to a maximum displacement of 0.1 Å at each time-step.

In MD simulations, the most time-consuming interactions are the nonbonded potentials, *i.e.* the van der Waals excluded-volume U_{vdw} (Eq. (5)) and the electrostatic interactions U_{coul} (Eq. (6)). Lyulin and coworkers have shown that U_{coul} can be switched off during the generation of glassy chains [8]. In addition, the Lennard Jones (LJ) form for U_{vdw} (Eq. (5)) can be replaced under certain conditions by the purely repulsive Weeks-Chandler-Andersen (WCA) form (Eq. (9)):

$$\begin{aligned} U_{\text{vdw}}(r) &= U_{\text{WCA}}(r) = 4\varepsilon \left(\left(\frac{\sigma}{r} \right)^{12} - \left(\frac{\sigma}{r} \right)^{6} \right) + \varepsilon \quad \text{when r} \leq 2^{1/6}\ \sigma \\ U_{\text{vdw}}(r) &= U_{\text{WCA}}(r) = 0 \qquad\qquad\qquad\qquad\quad \text{when r} > 2^{1/6}\ \sigma \end{aligned} \tag{9}$$

since it has already been shown using PMC-MD sampling that some rigid polymer configurations are mostly governed by the repulsive vdw interactions [18]. However, to ensure that it is the case for the polyimides under study, PMC-MD sampling was carried out for 50 ns while applying different conditions for the non-bonded potentials, *i.e.* either (i) the normal U_{LJ} and U_{coul} combination, (ii) the U_{LJ} on its own, or (iii) the U_{WCA} on its own. Table 1 reports the average radii of gyration for the chains and shows clearly that, as expected, the short-range WCA potential can safely be used here in place of the LJ and electrostatic form when configurations are being prepared.

Table 1. The PMC-MD single-chain sampled average radii of gyration along with their standard error using different combinations of non-bonded potentials

	PI1	**PI2**	**PI3**
Number of monomers	10	10	13
Number of atoms	662	662	730
Sampling temperature / K	650	600	700
$\langle S^2 \rangle^{1/2}$ with U_{LJ} and U_{coul} / Å	26±3	23±3	25±4
$\langle S^2 \rangle^{1/2}$ with U_{LJ} only / Å	26±4	22±3	26±4
$\langle S^2 \rangle^{1/2}$ with U_{WCA} only / Å	26±3	22±3	25±4

This approximation will not work for all properties [9, 10] but when its validity is confirmed [8, 18, 65], as shown in Table 1, it can very significantly speed-up the calculations.

The experimental densification was mimicked by gradually reducing x_{wall} on both sides until the central part of the system regained the density of the bulk. The walls were designed to move in response to the difference between the actual average pressure on the walls, P_{wall}, and a preset target value, P_{target}, using a loose-coupling algorithm [66]. It was found that compressing with the full U_{LJ} and U_{coul} non-bonded potentials amounted to pushing the rigid chains with, similarly to Fig. 1, very little mobility for them to rearrange at the interface. High temperatures did not improve much the situation either (results not shown). On the other hand, the purely repulsive U_{WCA} (Eq. (9)) can be used in place of U_{LJ} + U_{coul} (Table 1). To define P_{target}, each isotropic bulk was run at 308 K for 5 ns under constant-volume *NVT* conditions with all non-bonded potentials being replaced by U_{WCA}. The resulting average pressures of ~6075 bar for PI1, ~6170 bar for PI2 and ~5575 bar for PI3 were thus used as the respective P_{target} for the wall compression step.

At the start of the compression stage, the walls are too far from the polymer to interact. Since the polymer is surrounded by two empty spaces and U_{WCA} leads to an initial repulsion of the chains, there is a slight loss of cohesion along the *x*-direction. Providing that this effect remains limited, it has the major advantage of improving the local mobility while still maintaining the global configurations. As such, this extra space in the *x*-direction makes it easier for the polymer to rearrange at the interface. Several coupling constants were tested and a good compromise between the walls moving fast enough to avoid too much loss of the polymer cohesion while giving enough time for the chains at the interfaces to rearrange was found to be 0.1 ps. It took typically ~50 ps for the walls to compress the central region back to its initial bulk density. At the same time, too much heating was avoided by keeping the temperature at 308 K with a loose-coupling constant of 0.01 ps. The progressive advance of the left wall (from -100 Å to ~-50 Å along *x*) and the associated changes in the symmetrized P_{wall} pressure with respect to P_{target} are displayed for PI1 in Fig. 5 (a). Figs. 5 (b-c) show the behaviour of the symmetrized polymer mass densities averaged over *x*-slabs of 2 Å and some snapshots for the same system at various times into the compression.

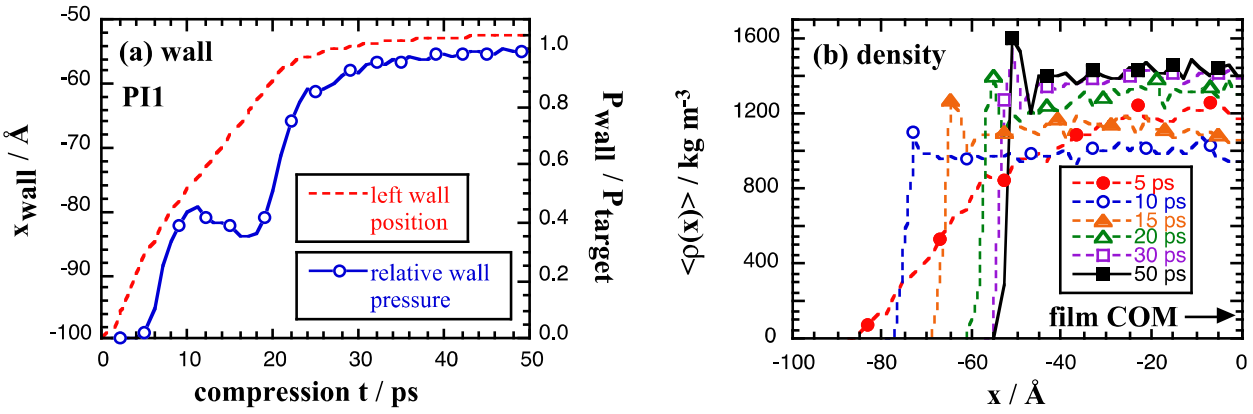

(c)

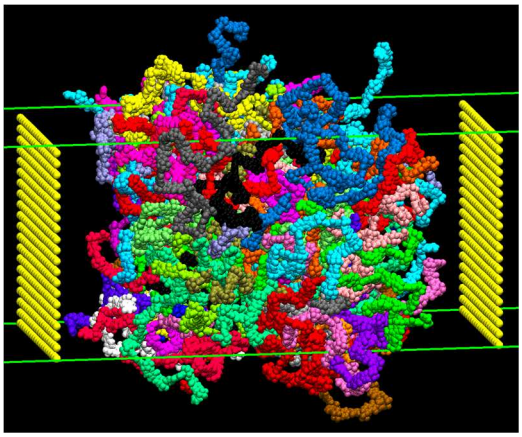

compression t = 0 ps

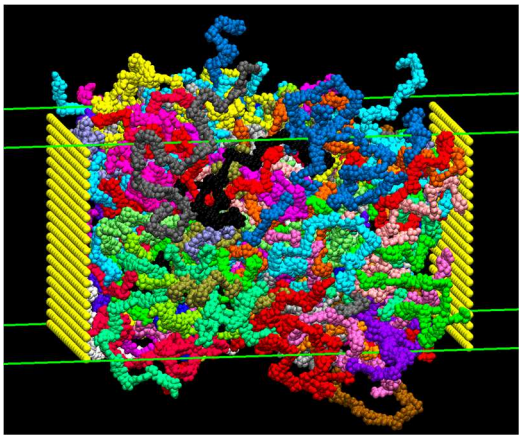

compression t = 5 ps

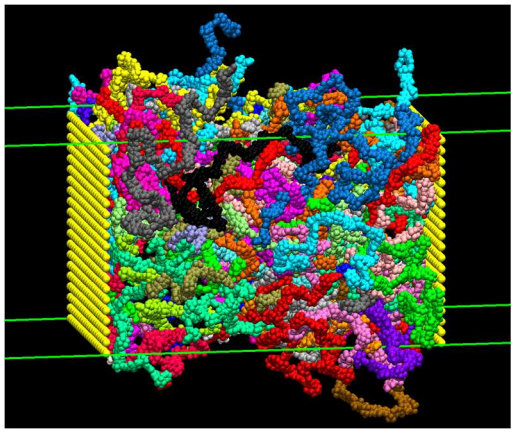

compression t = 10 ps

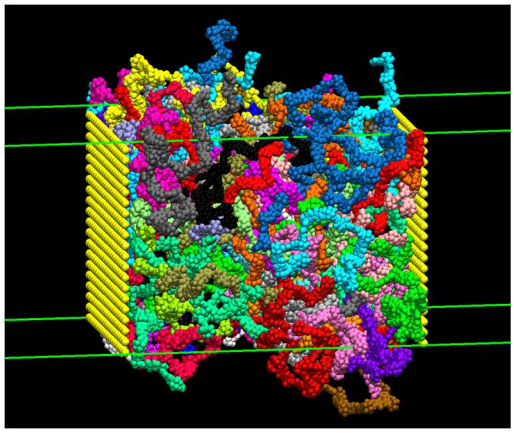

compression t = 15 ps

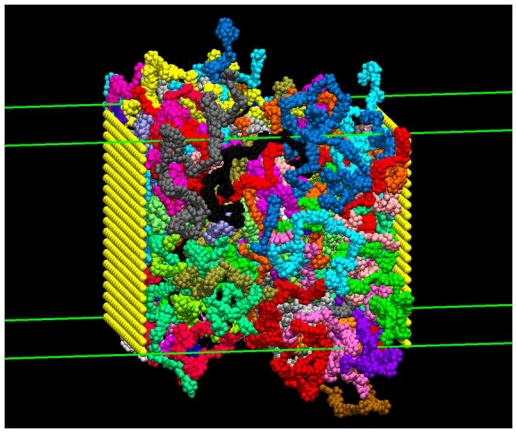

compression t = 20 ps

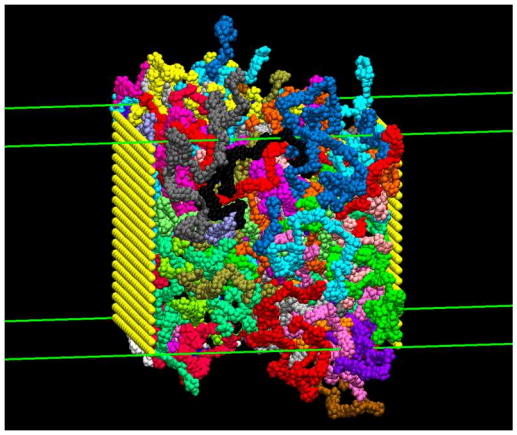

compression t = 30 ps

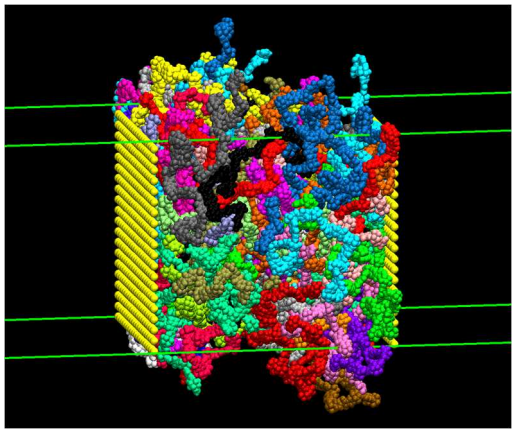

compression t = 50 ps

Fig. 5. Wall compression. **(a)** The position of the left wall as it moves towards the PI1 polymer (left axis) and the associated changes in wall pressure P_{wall} with respect to P_{target} (right axis) as a function of the compression time. **(b)** average symmetrized x-slab polymer mass densities $\langle\rho(x)\rangle$ and **(c)** snapshots of PI1 (with the wall being displayed here as a plane of yellow "atoms") at successive compression times.

The initial loss of polymer cohesion due to U_{WCA} is clear to see at $t = 5$ ps (Figs. 5 (b-c)) and, as expected, it corresponds to a negligeable P_{wall} (Fig. 5 (a)). A visual comparison of the configurations at $t = 0$ and $t = 5$ ps (Fig. 5 (c)) confirms that the central part of the model is hardly changed. Once the wall starts interacting with the polymer, P_{wall} increases and the expanded polymer gets pushed back. The first plateau in the pressure, i.e. up to $t = 20$ ps (Fig. 5 (a)), is related to the re-densification stage (Fig. 5 (b)), in which the polymer has enough mobility to adapt to the compression by modifying its local structure at the interface. At later compression times, its density gets closer to the bulk value, and as a result, its compressibility decreases significantly. P_{wall} thus increases sharply and P_{target} is reached around $t = 50$ ps.

The re-densification stage was found to be associated to local conformational and configurational chain rearrangements along the x-direction. This is illustrated for PI1 by Fig. 6, which displays the evolution of the $\langle P_2(\cos\theta_{\square})\rangle$ Legendre polynomials for the pivot Cket-N-Car linkers (Fig. 6 (a)) and the perpendicular components $\langle S_{\perp}^2(x)\rangle_{\square\square\square}$ the mean-square radii of gyration (Fig. 6 (b)), both as a function of x and for various successive compression times.

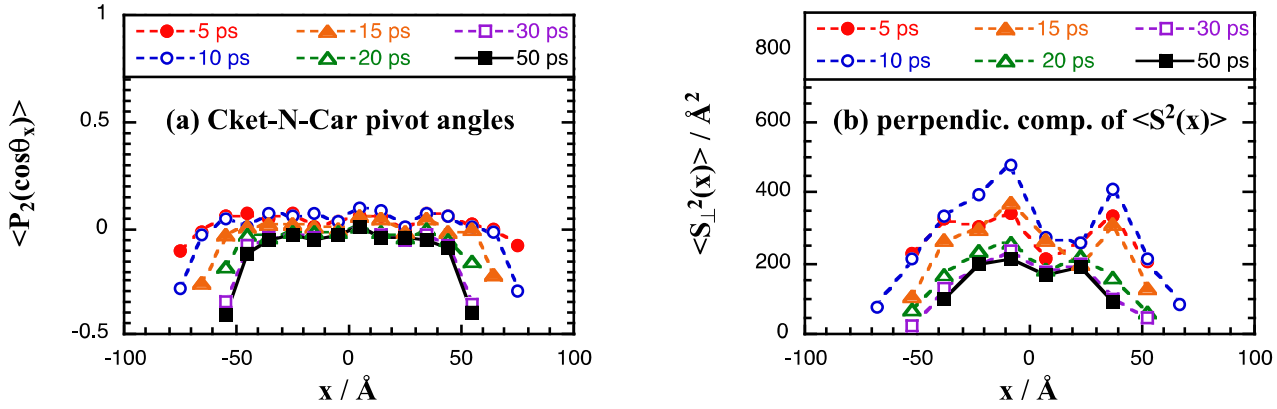

Fig. 6 PI1 *x*-slab evolution as a function of the compression time for **(a)** the pivot Cket-N-Car $\langle P_2(\cos\theta_x)\rangle$ and **(b)** the $\langle S_\perp^2(x)\rangle$ component of the mean-square radii of gyration.

Fig. 6 (a) shows that the pivot angles on both sides of the polymer tend to align in a parallel way with respect to the surfaces. This effect is very pronounced at the vicinity of the interfaces, where the θ_x angles are almost perfectly parallel to the surface, *i.e.* $\langle P_2(\cos\theta_x)\rangle \approx -0.5$, but it progressively gets attenuated within a distance of ~20 Å and does not affect the core of the model. Similarly, the decrease of $\langle S_\perp^2(x)\rangle$ at the vicinity of the interfaces indicates that the chains are flattened in these regions, whereas they remain similar to the bulk around the film COM (see Fig. 4). We note that the $S_\perp^2(x)\rangle$ component tends to becomes quite small as the wall advances but that it relaxes back to about 50% of the middle value at the end of the 50-ps compression phase. Interestingly, this compares quite favourably to values of 60% obtained by Aoyagi et al. [50] for bead-spring models of equilibrium polymer melts confined between walls. However, such results have been shown to depend on factors such as the stiffness of the chains [27, 49], so it is difficult to compare models which do not have the same force-fields.

The tendency of surface chains to be aligned and flattened with respect to the surfaces is well-known in polymer films and this behaviour has previously been referred to as "pancakes structures" [27, 49, 67-69]. However, unlike our former works with longer chains [2, 24-26], these specific features do not persist in the film cores. Our optimisation of the chain-lengths and the wall-compression procedure results in the central chains remaining similar to bulk chains.

The same analyses were carried out on slabs along the transversal *y* and *z* axes, but no significant alignments of the pivot angles and no flattenings of the chains were found along these directions (results

not shown). The changes in the local chain structures are thus mostly restricted to the longitudinal *x*-direction.

2.5. Relaxation and re-introduction of the full potential in the presence of the walls

Following the 50 ps-compression, the simulations were carried on with U_{WCA} and with the walls remaining fixed in place under *NVT* conditions for 5 ns at 308 K, which allowed for all the energies to stabilize. The systems were subsequently warmed up to their sampling temperatures just above the glass transition (Table 1) in order for the local stresses to relax better whilst the walls maintained the global cohesion. At this stage, the heat bath loose-coupling constant was reset to its standard value of 0.1 ps. Following 30 ns with the highly efficient $U_{WCA,}$ the full U_{LJ} and U_{coul} nonbonded potentials were then re-introduced and the high-temperature runs continued for 3 ns to allow for local relaxation under these new conditions. We note that this high-temperature step in the presence of the walls is not really intended to mimick an experimental procedure. It simply gives more mobility for the model chains to relax locally at the interface, without any risk of losing the cohesion in the middle of the film. The polymer+walls systems were cooled back to 308 K at a rate of -1 K ps^{-1} and allowed to stabilize for at least 1 ns.

Fig. 7 displays the $\langle P_2(\cos\theta_{\square}) \rangle$ for the pivot Cket-N-Car angle (Fig. 7 (a)) and the perpendicular components $\langle S_{\perp}^2(x) \rangle_{\square\square\square}$ the mean-square radii of gyration (Fig. 7 (b)) in PI2, both as a function of *x* and at various steps during the relaxation procedure. It is clear that the parameters of the optimized relaxation procedure (temperatures, stabilization times, cooling rates) do not affect the conformational and configurational features created by the compression

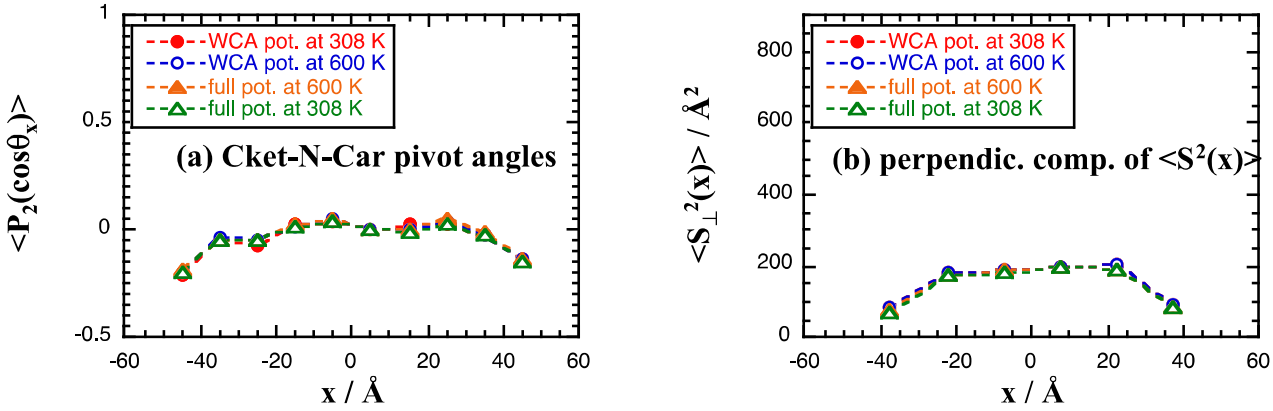

Fig. 7 PI2 *x*-slab evolution as a function of the relaxation steps for **(a)** the pivot Cket-N-Car $\langle P_2(\cos\theta_x)\rangle$ and **(b)** the $\langle S_\perp^2(x)\rangle$ component of the mean-square radii of gyration.

2.6. Removal of the walls and final model films

In this last stage, x_{wall} was instantaneously reset to ±150 Å, thus creating two empty reservoirs of ~(100 Å)^3 on each side of the polymer film. Following a short *NVT* relaxation, the systems were then switched for 10 ns to specific *NPT* conditions in which only the transversal *P*yy and *P*zz components of the pressure tensor, ***P***, were maintained close to 1 bar by loose-coupling to the *y* and *z* box lengths, respectively. The loose-coupling relaxation time for the pressure was set to 5 ps [66]. The *x*-box lengths remained fixed at 300 Å. This condition allowed for the surface areas of the glassy films to relax while keeping the MD boxes orthorhombic. PI3 is the lowest-density polyimide under study, and as such, is the most likely to relax significantly. Its transversal pressure typically relaxes within a few ns, and results in the *y*-box and *z*-box dimensions changing by less than 2 Å (Fig. 8, triangles). Indeed, the average relaxed *y*-box length of 98.67±0.02 is close to the average relaxed *z*-box length of 98.96±0.01.

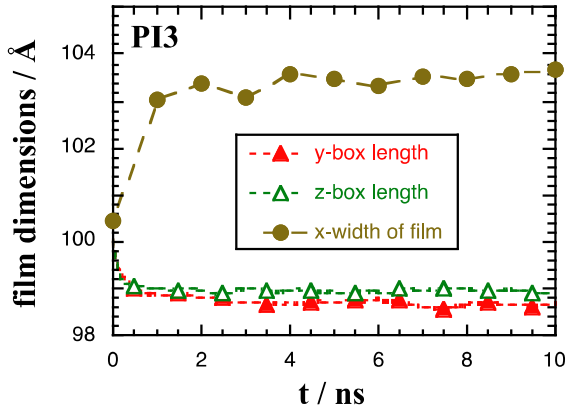

Fig. 8 Relaxation of the PI3 film surface areas (box lengths along the *y*-axis and *z*-axis) and its width in the *x*-direction upon removal of the walls.

To assess the structural width along the longitudinal *x*-direction, the symmetrized polymer $\rho(x)$ mass-density curves were fitted at various times to the following equation [70, 71]:

$$\rho(x) = \rho_{middle} \frac{1 - \tanh\left[2\left(x-h\right)/w\right]}{2} \tag{10}$$

with ρ_{middle} being the density in the central region of the film, h being the location of the interface (with respect to the membrane COM) and w being the width of the interface. The *x*-width of the membrane can then be defined as $2h$ and is displayed for PI3 in Fig. 8 (circles) along with the other dimensions. The maximum relaxation in the *x*-direction is less than 4%, which remains very limited. For the denser PI1 and PI2 polyimides, it was found to be less than 1.5%. The chain dynamics were characterized by analysing the mean-square displacements, MSD = $\langle(\mathbf{r}_i(t+t_0)-\mathbf{r}_i(t_0))^2\rangle$, with $\boldsymbol{r}_i$ being the position of atom *i*, t_0 being a time-origin and *t* being a preset time-interval. The MSDs were averaged over all polymer atoms and over all time-origins considered and, as for the conformational and configurational analyses, they were resolved in *x*-slabs of width 10 Å.

Fig. 9 displays the densities (Fig. 9 (a)), conformational (Fig. 9 (b)), configurational (Fig. 9 (c)) and dynamical (Fig. 9 (d)) characteristics of the glassy model films, averaged over the last 5 ns of the simulations. They can be compared directly with the corresponding values for the isotropic bulks (Fig. 4).

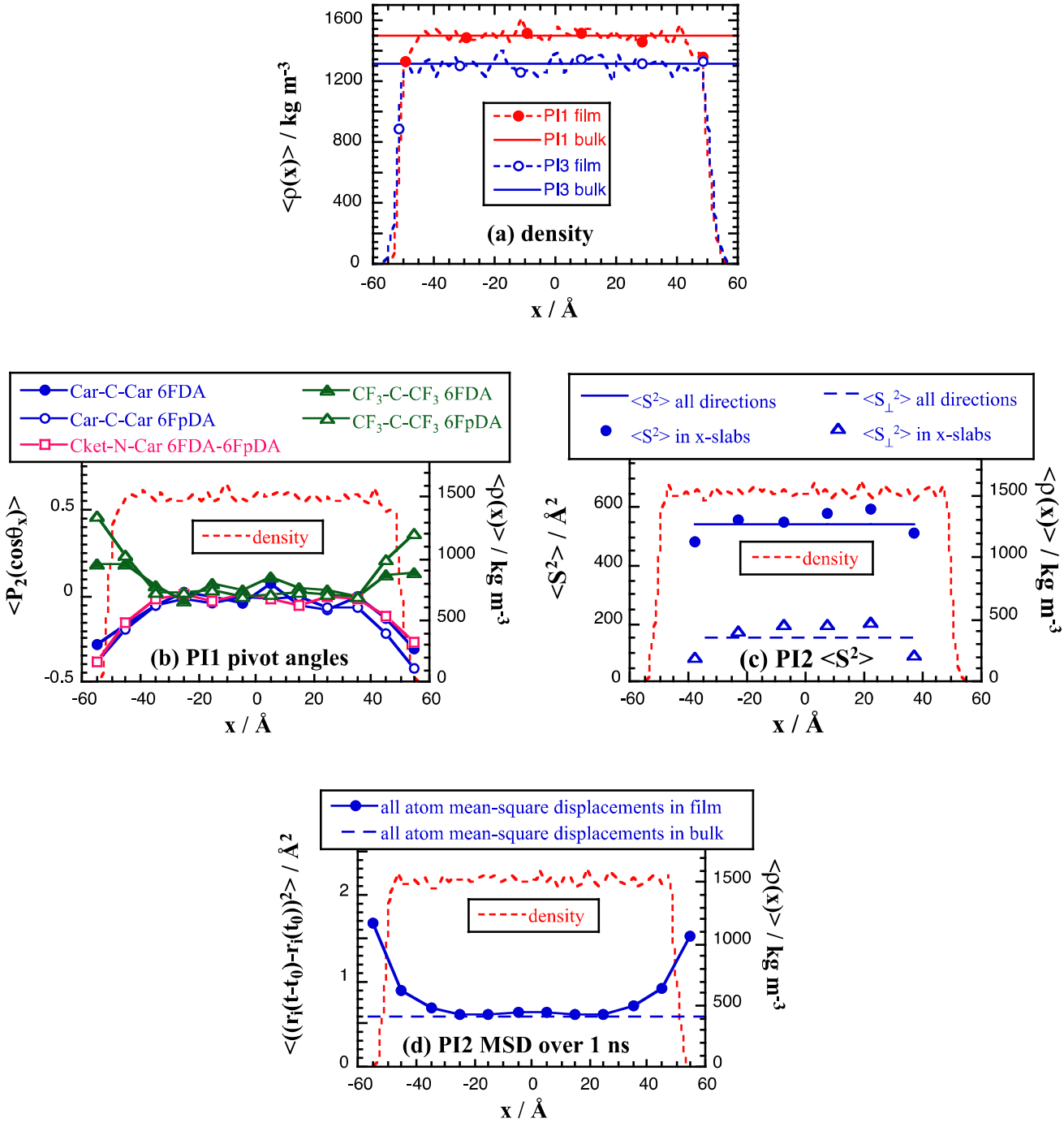

Fig. 9. **(a)** The PI1 and PI3 films *x*-slab mass densities $\langle\rho(x)\rangle$ compared to their isotropic bulk values **(b-d)** Left axes with their x-slab resolutions: **(b)** the $\langle P_2(\cos\theta_x)\rangle$ for the pivot angles in the PI1 film. **(c)** The $\langle S^2\rangle$ and $\langle S_\perp{}^2(x)\rangle$ for the PI2 film **(d)** the polymer MSDs for the PI2 film averaged over a $t = 1$ ns time-interval. Also shown for comparison in **(b-d)** are the respective *x*-slab mass densities (right axes).

From the above analyses, it is clear that the chains remain isotropic and bulk-like in the middle of the model films (Fig. 9 (a)). On the other hand, the ring-ring Car-C-Car and C-N-C pivot angles at the vicinity of the interface are now parallel to the surface (Fig. 9 (b)), and the CF_3-C-CF_3 angles settle as expected in a perpendicular way to the direction of the main backbone. The lower $\langle S_{\perp}^2(x) \rangle$ also confirm that the chains remain flattened in the interfacial regions (Fig. 9 (c)). In terms of mobility, the MSDs averaged over a 1 ns time-interval are less than 1 $Å^2$ and similar to the bulk in the middle of the film (Fig. 9 (d)). This is agreement with glassy polymers and their "immeasurably small chain self-diffusivities" [33]. Even if the local diffusivity is known to slightly increases at the free polymer surfaces [32], Fig. 9 (d) shows that it remains very small, and as such, that the cohesion of both interfaces are preserved. Following the removal of the wall, the relaxed glassy film models are thus able to conserve their bulk-like characteristics in the core and their surface-like characteristics in the vicinity of the interfaces.

As explained above, the structural width of these polyimide membranes can be characterized by fitting Eq. (10) to the $\rho(x)$ mass-density curves of Fig. 9 (a). The fitted densities in the middle of the films are found to be ρ_{middle} = 1499.0, 1520.6 and 1311.4 kg m^{-3} for PI1, PI2 and PI3, respectively, which are almost identical to the isotropic bulk densities (Section 2.3.). In the same order, the 2□-defined widths of the membranes are 101.5, 101.1 and 103.5 Å, while the widths of the interfaces, defined as 2w, are 6.9, 5.5 and 7.5 Å. This latter parameter, which only uses the density as input, is probably underestimated. Indeed, it is well known that in such free-standing film models, the location and the width of the interfaces depend both on the property and on the way it is analyzed [22-25, 42]. Fig. 9b-c suggest much larger interfacial widths of ~20 Å on each side, with cores of ~60 Å. These are confirmed by the dynamical interfacial widths obtained while resolving the polymer atom MSDs in x-slabs, which are also of the order of ~20 Å (Fig. 9d). In these systems, the influence of an interface thus extends over a distance similar to the average radius of gyration of the chains.

Fig. 10 provides several visual representations of the three polyimide films under study. Fig. 10 (a) shows three selected molecules in the PI1 film ranging from the left to the right interface. The flattened and parallel orientation to the surfaces is clear to see for both molecules at the edges of the film. Fig. 10 (b-c) compare the longitudinal (Fig. 10 (b)) and transversal (Fig. 10 (c)) arrangements of the

chains in the PI2 film. There again, the transversal representation shows the specific "pancake" features at the surface. The full simulation box for the PI3 film is given in Fig. 10 (c).

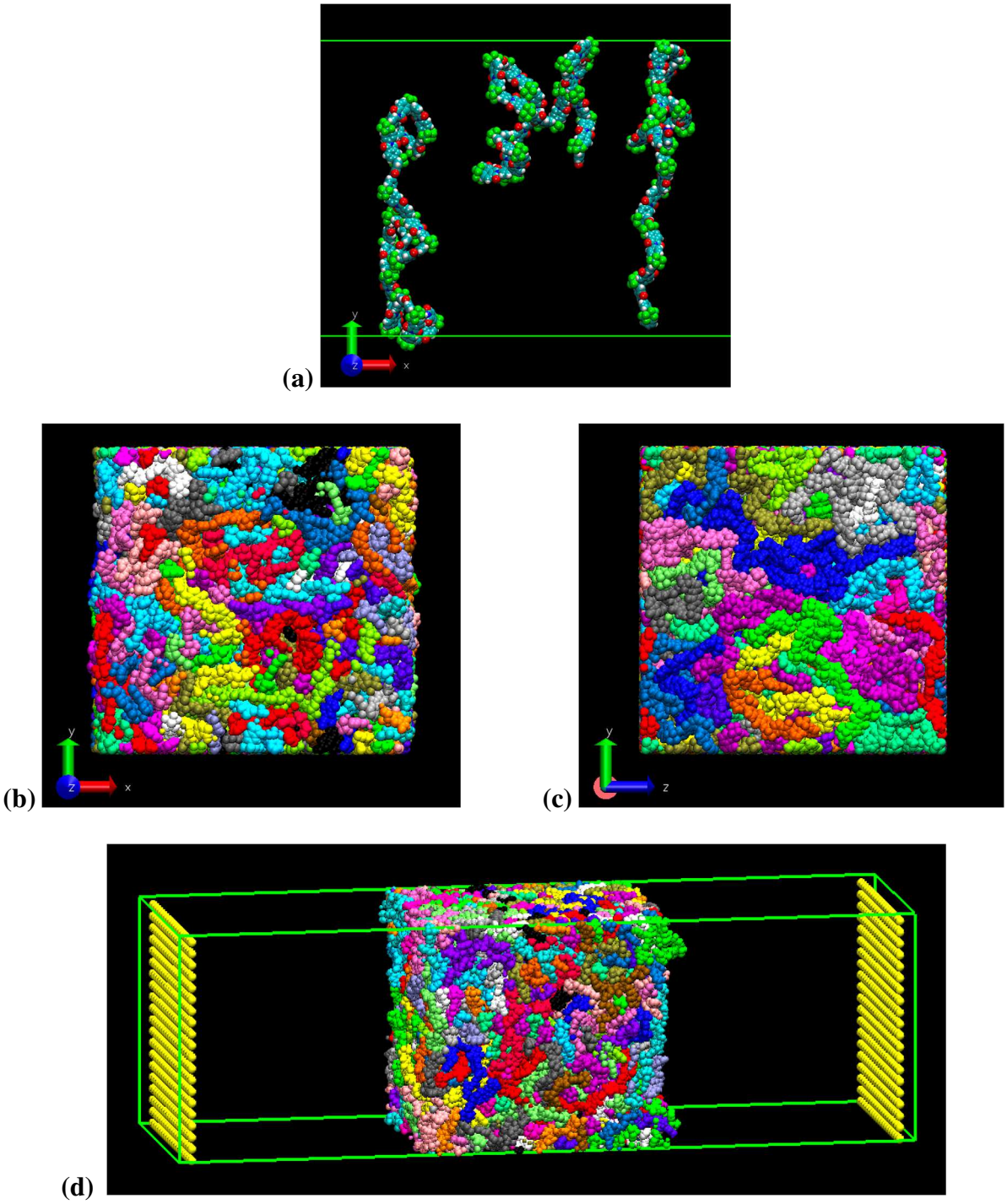

Fig. 10. Schematic representations of the three polyimide films under study. **(a)** Three molecules in the PI1 film including one from the left interface, one from the middle of the film and one from the right interface. The color code for the atom-types is cyan = C, red = O, blue = N, white = H, green = F. **(b) and (c)** The PI2 film along the longitudinal **(b)** and transversal **(c)** directions. **(d)** The entire PI3 simulation box with the reservoirs on either side of the film. In (b-d), the atoms have been folded back into their primary box and the different colours refer to different chains.

In terms of computing resources, ~15000 CPU hours were necessary to prepare each membrane of ~80000 atoms on either 18 or 27 processors. The PMC-MD and WCA parts of the procedure accounted for less than 2% of the resources used. Inevitably for simulations using a full explicit-atom potential (Eq. (1)), most of the time is spent calculating the van der Waals and electrostatic interactions. As noted before, these are very large systems and such simulations are much more expensive computationally than coarse-grained ones.

3. Conclusions

An optimized explicit-atom wall-compression procedure to generate models of glassy polymer films containing both surface-like and bulk-like chains for use in MD simulations has been developed. Starting from an isotropic bulk model, the *x*-dimension of the simulation box is first expanded and flat walls are placed on both sides at a distance initially far enough to avoid any interactions with the polymer chains. Densification is then successfully achieved by compressing the polymer with the walls until the central region regains the density of the bulk. It has been shown that using a purely repulsive van der Waals potential during the compression phase gives sufficient mobility to the polymer chains for them to rearrange at the interfaces. A subsequent heat treatment above the glass transition temperature followed by the reintroduction of the full potentials and cooling leads to stable films with clearly-defined interfaces.

The densities, conformations and configurations of the chains were monitored at each step of the preparation. The compression stage with the purely repulsive potential was found to be associated to rearrangements along the *x*-direction, with the surface chains becoming aligned and flattened with respect to the surfaces. On the other hand, the bulk chains in the centre of the models remained unaffected. Our glassy film models thus combine bulk-like characteristics in their centre and surface-like characteristics in the vicinity of the interfaces. In terms of sizes, it is recommended that the average radius of gyration of the chains is at least four times smaller than the desired width of the model membrane, and that the dimensions of the system in the transversal directions are similar to that in the longitudinal one in order to avoid any edge-effect artefacts. In the present case, an average radius of gyration of ~25 Å for the glassy chains leads to models with an isotropic core of ~(60×100×100) $Å^3$ and two interfacial regions amounting to a total of ~(40×100×100) $Å^3$. Their reservoirs on either sides (Fig. 10 (d)) make them especially suited

to study the sorption and diffusion of small molecules through the glassy films, which are at the basis of gas separations by polymer membranes (for a recent Review, see Ref. [72]).

Acknowledgments

This work was performed within the frameworks of the Institute for Sustainable Process Technology (www.ispt.eu) and the Centre of Excellence of Multifunctional Architectured Materials "CEMAM" n° ANR-10-LABX-44-01. It was granted access to the HPC resources of CCRT/CINES/IDRIS under the allocations 2018-095053 and 2019-095053 made by GENCI (Grand Equipement National de Calcul Intensif), France. The University Savoie Mont Blanc - CNRS/IN2P3 MUST computing centre, France, is also acknowledged for the provision of computer time.

Data Availability

The data that support the findings of this study are available upon request from the corresponding author.

References

[1] T.E. Gartner III, A. Jayaraman, Modeling and simulations of polymers: A roadmap, Macromolecules, 52 (2019) 755-786. https://doi.org/10.1021/acs.macromol.8b01836
[2] S. Neyertz, D. Brown, Air sorption and separation by polymer films at the molecular level, Macromolecules, 51 (2018) 7077-7092. https://doi.org/10.1021/acs.macromol.8b01423
[3] P.C. Tan, B.S. Ooi, A.L. Ahmad, S.C. Low, Monomer atomic configuration as key feature in governing the gas transport behaviors of polyimide membrane, J. Appl. Polym. Sci., 135 (2017) 46073. https://doi.org/10.1002/app.46073
[4] M.P. Allen, D.J. Tildesley, Computer simulation of liquids, Clarendon Press, Oxford, U.K., 1987.
[5] K.D. Hammonds, J.-P. Ryckaert, On the convergence of the SHAKE algorithm, Comput. Phys. Commun., 62 (1991) 336-351. https://doi.org/10.1016/0010-4655(91)90105-T
[6] G. Ciccotti, M. Ferrario, J.P. Ryckaert, Molecular dynamics of rigid systems in cartesian coordinates. A general formulation, Mol. Phys., 47 (1982) 1253 - 1264. https://doi.org/10.1080/00268978200100942
[7] P.P. Ewald, Die berechnung optischer und elektrostatisher gitterpotentiale, Ann. Phys., 369 (1921) 253-287. https://doi.org/10.1002/andp.19213690304
[8] S.V. Lyulin, A.A. Gurtovenko, S.V. Larin, V.M. Nazarychev, A.V. Lyulin, Microsecond atomic-scale molecular dynamics simulations of polyimides, Macromolecules, 46 (2013) 6357-6363. https://doi.org/10.1021/ma4011632
[9] S.V. Lyulin, S.V. Larin, A.A. Gurtovenko, V.M. Nazarychev, S.G. Falkovich, V.E. Yudin, V.M. Svetlichnyi, I.V. Gofman, A.V. Lyulin, Thermal properties of bulk polyimides: Insights from computer modeling versus experiment, Soft Matter, 10 (2014) 1224-1232. https://doi.org/10.1039/c3sm52521j
[10] S.G. Falkovich, S.V. Lyulin, V.M. Nazarychev, S.V. Larin, A.A. Gurtovenko, N.V. Lukasheva, A.V. Lyulin, Influence of the electrostatic interactions on the thermophysical properties of

polyimides: Molecular-dynamics simulations, J. Polym. Sci., Part B: Polym. Phys., 52 (2014) 640-646. https://doi.org/10.1002/polb.23460
[11] M. Balçik, M.G. Ahunbay, Prediction of CO_2-induced plasticization pressure in polyimides via atomistic simulations, J. Membr. Sci., 547 (2018) 146-155. https://doi.org/10.1016/j.memsci.2017.10.038
[12] S.S.M. Lock, K.K. Lau, A.M. Shariff, Y.F. Yeong, M.A. Bustam, Thickness dependent penetrant gas transport properties and separation performance within ultrathin polysulfone membrane: Insights from atomistic molecular simulation, J. Polym. Sci., Part B: Polym. Phys., 56 (2018) 131-158. https://doi.org/10.1002/polb.24523
[13] M. Mazo, N. Balabaev, A. Alentiev, Y. Yampolskii, Molecular dynamics simulation of nanostructure of high free volume polymers with $SiMe_3$ side groups, Macromolecules, 51 (2018) 1398-1408. https://doi.org/10.1021/acs.macromol.7b02470
[14] H. Lei, S. Qi, D. Wu, Hierarchical multiscale analysis of polyimide films by molecular dynamics simulation: Investigation of thermo-mechanical properties, Polymer, 179 (2019) 121645. https://doi.org/10.1016/j.polymer.2019.121645
[15] J.D. Ferry, Viscoelastic properties of polymers, 3rd ed., Wiley, New York, 1980.
[16] R.P. Chartoff, B. Maxwell, Dynamic mechanical properties of polymer melts: The dependence of viscoelastic properties on molecular weight distribution, Polym. Eng. & Sci., 9 (1969) 159-163. https://doi.org/10.1002/pen.760090303
[17] O. Hölck, M. Böhning, M. Heuchel, M.R. Siegert, D. Hofmann, Gas sorption isotherms in swelling glassy polymers - detailed atomistic simulations, J. Membr. Sci., 428 (2013) 523-532. https://doi.org/10.1016/j.memsci.2012.10.023
[18] S. Neyertz, D. Brown, Influence of system size in molecular dynamics simulations of gas permeation in glassy polymers, Macromolecules, 37 (2004) 10109-10122. https://doi.org/10.1021/ma048500q
[19] S. Pandiyan, D. Brown, N.F.A. Van der Vegt, S. Neyertz, Atomistic models of three fluorinated polyimides in the amorphous state, J. Polym. Sci., Part B: Polym. Phys., 47 (2009) 1166-1180. https://doi.org/10.1002/polb.21717
[20] C. Rizzuto, A. Caravella, A. Brunetti, C.H. Park, Y.M. Lee, E. Drioli, G. Barbieri, E. Tocci, Sorption and diffusion of CO_2/N_2 in gas mixture in thermally-rearranged polymeric membranes: A molecular investigation, J. Membr. Sci., 528 (2017) 135-146. https://doi.org/10.1016/j.memsci.2017.01.025
[21] S. Neyertz, A. Douanne, D. Brown, A molecular dynamics simulation study of surface effects on permeation in free-standing polyimide membranes, J. Membr. Sci., 280 (2006) 517-529. https://doi.org/10.1016/j.memsci.2006.02.011
[22] S. Neyertz, D. Brown, Molecular dynamics simulations of oxygen transport through a fully atomistic polyimide membrane, Macromolecules, 41 (2008) 2711-2721. https://doi.org/10.1021/ma7026676
[23] S. Neyertz, D. Brown, Oxygen sorption in glassy polymers studied at the molecular level, Macromolecules, 42 (2009) 8521-8533. https://doi.org/10.1021/ma901478d
[24] S. Neyertz, D. Brown, The effect of structural isomerism on carbon dioxide sorption and plasticization at the interface of a glassy polymer membrane, J. Membr. Sci., 460 (2014) 213-228. https://doi.org/10.1016/j.memsci.2014.03.002
[25] S. Neyertz, D. Brown, Molecular dynamics study of carbon dioxide sorption and plasticization at the interface of a glassy polymer membrane, Macromolecules, 46 (2013) 2433-2449. https://doi.org/10.1021/ma302073u
[26] S. Neyertz, D. Brown, Nanosecond-time-scale reversibility of dilation induced by carbon dioxide sorption in glassy polymer membranes, J. Membr. Sci., 520 (2016) 385-399. https://doi.org/10.1016/j.memsci.2016.08.003

[27] M. Vacatello, Monte Carlo simulations of the interface between polymer melts and solids. Effects of chain stiffness, Macromol. Theory Simul., 10 (2001) 187-195. https://doi.org/10.1002/1521-3919(20010301)10:3%3C187::AID-MATS187%3E3.0.CO;2-J
[28] P. Doruker, W.L. Mattice, Simulation of polyethylene thin films on a high coordination lattice, Macromolecules, 31 (1998) 1418-1426. https://doi.org/10.1021/ma971322z
[29] J. Chang, J. Han, L. Yang, R.L. Jaffe, D.Y. Yoon, Structure and properties of polymethylene melt surfaces from molecular dynamics simulations, J. Chem. Phys., 115 (2001) 2831-2840. https://doi.org/10.1063/1.1379536
[30] A.S. Ijantkar, U. Natarajan, Atomistic simulations of the structure and thermodynamic properties of poly(1,2-vinyl-butadiene) surfaces, Polymer, 45 (2004) 1373-1381. https://doi.org/10.1016/j.polymer.2003.09.067
[31] M. Soniat, M. Tesfaye, D. Brooks, B. Merinov, W.A. Goddard III, A.Z. Weber, F.A. Houle, Predictive simulation of non-steady-state transport of gases through rubbery polymer membranes, Polymer, 134 (2018) 125-142. https://doi.org/10.1016/j.polymer.2017.11.055
[32] K.F. Mansfield, D.N. Theodorou, Molecular dynamics simulation of a glassy polymer surface, Macromolecules, 24 (1991) 6283-6294. https://doi.org/10.1021/ma00023a034
[33] J.-L. Barrat, J. Baschnagel, A. Lyulin, Molecular dynamics simulations of glassy polymers, Soft Matter, 2010 (2010) 3430-3446. https://doi.org/10.1039/B927044B
[34] W. Humphrey, A. Dalke, K. Schulten, VMD: Visual molecular dynamics, J. Mol. Graphics, 14 (1996) 33-38. https://doi.org/10.1016/0263-7855(96)00018-5
[35] P. Doruker, W.L. Mattice, Effect of surface roughness on structure and dynamics in thin films, Macromol. Theory Simul., 10 (2001) 363-367. https://doi.org/10.1002/1521-3919(20010401)10:4%3C363::AID-MATS363%3E3.0.CO;2-V
[36] T.C. Clancy, J.H. Jang, A. Dhinojwala, W.L. Mattice, Orientation of phenyl rings and methylene bisectors at the free surface of atactic polystyrene, J. Phys. Chem. B, 105 (2001) 11493-11497. https://doi.org/10.1021/jp011588e
[37] V. Marcon, D. Fritz, N.F.A. van der Vegt, Hierarchical modelling of polystyrene surfaces, Soft Matter, 8 (2012) 5585-5594. https://doi.org/10.1039/C2SM25342A
[38] S. Queyroy, S. Neyertz, D. Brown, F. Müller-Plathe, Preparing relaxed systems of amorphous polymers by multiscale simulation: Application to cellulose, Macromolecules, 37 (2004) 7338-7350. https://doi.org/DOI: 10.1021/ma035821d
[39] A. Chakrabarty, T. Cagin, Coarse grain modeling of polyimide copolymers, Polymer, 51 (2010) 2786-2794. https://doi.org/10.1016/j.polymer.2010.03.060
[40] S. Pandiyan, P.V. Parandekar, O. Prakash, T. Tsotsis, S. Basu, Systematic coarse graining of a high-performance polyimide, Macromol. Theory Simul., 24 (2015) 513-520. https://doi.org/10.1002/mats.201500009
[41] S. Neyertz, A. Douanne, D. Brown, Effect of interfacial structure on permeation properties of glassy polymers, Macromolecules, 38 (2005) 10286-10298. https://doi.org/10.1021/ma051463y
[42] S. Neyertz, Tutorial: Molecular dynamics simulations of microstructure and transport phenomena in glassy polymers, Soft Mater., 4 (2007) 15-83. https://doi.org/10.1080/15394450601155608
[43] M. Tsige, G.S. Grest, Molecular dynamics study of the evaporation process in polymer films, Macromolecules, 37 (2004) 4333-4335. https://doi.org/10.1021/ma049509v
[44] J.H. Jang, W.L. Mattice, The effect of solid wall interaction on an amorphous polyethylene thin film, using a Monte Carlo simulation on a high coordination lattice, Polymer, 40 (1999) 4685-4694. https://doi.org/10.1016/S0032-3861(99)00071-3
[45] J.A. Torres, P.F. Nealey, J.J. De Pablo, Molecular simulation of ultrathin polymeric films near the glass transition, Phys. Rev. Lett., 85 (2000) 3221-3224. https://doi.org/10.1103/PhysRevLett.85.3221

[46] S. Peter, H. Meyer, J. Baschnagel, Thickness-dependent reduction of the glass-transition temperature in thin polymer films with a free surface, J. Polym. Sci., Part B: Polym. Phys., 44 (2006) 2951-2967. https://doi.org/10.1002/polb.20924
[47] K.F. Mansfield, D.N. Theodorou, Atomistic simulation of a glassy polymer surface, Macromolecules, 23 (1990) 4430-4445. https://doi.org/10.1021/ma00222a016
[48] K.F. Mansfield, D.N. Theodorou, Atomistic simulation of a glassy polymer/graphite interface, Macromolecules, 24 (1991) 4295-4309. https://doi.org/10.1021/ma00015a011
[49] M. Vacatello, Ordered arrangement of semiflexible polymers at the interface with solids, Macromol. Theory Simul., 11 (2002) 53-57. https://doi.org/10.1002/1521-3919(20020101)11:1%3C53::AID-MATS53%3E3.0.CO;2-N
[50] T. Aoyagi, J.-I. Takimoto, M. Doi, Molecular dynamics study of polymer melt confined between walls J. Chem. Phys., 115 (2001) 552-559. https://doi.org/10.1063/1.1377015
[51] M. Vacatello, Monte Carlo simulations of polymers in nanoslits, Macromol. Theory Simul., 13 (2004) 30-35.
[52] S. Neyertz, D. Brown, Preparation of bulk melt chain configurations of polycyclic polymers, J. Chem. Phys., 115 (2001) 708-717. https://doi.org/10.1063/1.1379073
[53] M.K. Ghosh, K.L. Mittal, in Polyimides: Fundamentals and Applications, Marcel Dekker, Inc., New York, 1996.
[54] D. Brown, The gmq User Manual Version 5: available at http://www.lmops.univ-savoie.fr/brown/gmq.html, (2013).
[55] M. Clark, R.D. Cramer III, N. Van Opdenbosch, Validation of the general purpose Tripos 5.2 force field, J. Comput. Chem., 10 (1989) 982-1012. https://doi.org/10.1002/jcc.540100804
[56] S. Pandiyan, D. Brown, S. Neyertz, N.F.A. Van der Vegt, Carbon dioxide solubility in three fluorinated polyimides studied by molecular dynamics simulations, Macromolecules, 43 (2010) 2605-2621. https://doi.org/10.1021/ma902507d
[57] S. Neyertz, D. Brown, S. Pandiyan, N.F.A. Van der Vegt, Carbon dioxide diffusion and plasticization in fluorinated polyimides, Macromolecules, 43 (2010) 7813-7827. https://doi.org/10.1021/ma1010205
[58] M. Lal, Monte Carlo computer simulation of chain molecules. I, Mol. Phys., 17 (1969) 57-64. https://doi.org/10.1080/00268976900100781
[59] P.J. Flory, The statistical mechanics of chain molecules, Hanser Publishers, New York, 1988.
[60] D.N. Theodorou, U.W. Suter, Detailed molecular structure of a vinyl polymer glass, Macromolecules, 18 (1985) 1467-1478. https://doi.org/10.1021/ma00149a018
[61] M.R. Coleman, W.J. Koros, The transport properties of polyimide isomers containing hexafluoroisopropylidene in the diamine residue, J. Polym. Sci., Part B: Polym. Phys., 32 (1994) 1915-1926. https://doi.org/10.1002/polb.1994.090321109
[62] D. Hofmann, M. Heuchel, Y. Yampolskii, V. Khotimskii, V. Shantarovich, Free volume distributions in ultrahigh and lower free volume polymers: Comparison between molecular modeling and positron lifetime studies, Macromolecules, 35 (2002) 2129-2140. https://doi.org/10.1021/ma011360p
[63] H.J.C. Berendsen, J.P.M. Postma, W.F. Van Gunsteren, A. DiNola, J.R. Haak, Molecular dynamics with coupling to an external bath, J. Chem. Phys., 81 (1984) 3684-3690. https://doi.org/10.1063/1.448118
[64] D. Barbier, D. Brown, A.-C. Grillet, S. Neyertz, Interface between end-functionalized peo oligomers and a silica nanoparticle studied by molecular dynamics simulations, Macromolecules, 37 (2004) 4695-4710. https://doi.org/DOI: 10.1021/ma0359537
[65] V.M. Nazarychev, A.V. Lyulin, S.V. Larin, A.A. Gurtovenko, J.M. Kenny, S.V. Lyulin, Molecular dynamics simulations of uniaxial deformation of thermoplastic polyimides, Soft Matter, 12 (2016) 3972-3981. https://doi.org/10.1039/C6SM00230G

[66] D. Brown, J.H.R. Clarke, A loose-coupling constant pressure molecular dynamics algorithm for use in the modelling of polymer materials, Comput. Phys. Commun., 62 (1991) 360-369. https://doi.org/10.1016/0010-4655(91)90107-V
[67] I. Bitsanis, G. Hadziioannou, Molecular dynamics simulations of the structure and dynamics of confined polymer melts, J. Chem. Phys., 92 (1990) 3827-3847. https://doi.org/10.1063/1.457840
[68] C. Mischler, J. Baschnagel, K. Binder, Polymer films in the normal-liquid and supercooled state: A review of recent monte carlo simulation results, Adv. Colloid Interface Sci., 94 (2001) 197-227. https://doi.org/10.1016/s0001-8686(01)00061-6
[69] S. Izumisawa, M.S. Jhon, Molecular simulation of thin polymer films with functional endgroups, J. Chem. Phys., 117 (2002) 3972-3977. https://doi.org/10.1063/1.1494426
[70] E. Helfand, Y. Tagami, Theory of the interface between immiscible polymers. II, J. Chem. Phys., 56 (1972) 3592-3601. https://doi.org/10.1063/1.1677735
[71] E. Helfand, Y. Tagami, Theory of the interface between immiscible polymers, J. Chem. Phys., 57 (1972) 1812-1813. https://doi.org/10.1063/1.1678491
[72] N. Vergadou, D.N. Theodorou, Molecular modeling investigations of sorption and diffusion of small molecules in glassy polymers, Membranes, 9 (2019) 98. https://doi.org/10.3390/membranes9080098